GPS Solutions (2023) 27:52
https://doi.org/10.1007/s10291-022-01387-0

ORIGINAL ARTICLE

Mixed QZSS/GPS/Galileo RTK positioning with a trade-off between ionosphere-weighting and ionosphere-fixed models: an ambiguity resolution method for Japan

Feng-Yu Chu[1,2] · **Nobuaki Kubo**[2] · **Yize Zhang**[2,3]

Received: 9 May 2022 / Accepted: 21 December 2022

Abstract
In real-time kinematic (RTK) positioning, the ambiguity resolution (AR) performance is critically affected by ionospheric delays. The ionospheric delays can be represented by a function of vertical total electron content values. Most of Japan is in mid-latitude regions, over which the spatial gradient of the vertical total electron content is usually small. Under the condition and after the highest pivot satellite is chosen, if more high-elevation secondary satellites are available, then the number of double-differenced (DD) measurements with small ionospheric delays (MSIDs) (e.g., < 10 cm) can increase within medium-long baselines. The mixed-constellation DD technique can produce measurements with more high-elevation secondary satellites than the classical DD technique, and at least one Quasi-Zenith Satellite System (QZSS) satellite can be constantly observed at elevations higher than 60° over the entire Japan. Therefore, the mixed-constellation DD technique, including QZSS, can make the number of DD MSIDs as large as possible in Japan. In the presence of more DD MSIDs, the AR can perform better on the premise that the ionospheric pseudo-observations are given properly. For the mixed QZSS/GPS/Galileo RTK positioning in Japan, this study proposes a cascading AR from high to low elevations to mitigate the occurrence of the improper provision of ionospheric pseudo-observations. In the analysis, the proposed and conventional AR methods are compared. The experimental results show that the success percentage of AR can improve by 41.7% and 6.3% for baselines 100 and 200 km, respectively.

Keywords QZSS · Mixed-constellation RTK · Ambiguity resolution

Introduction

Real-time kinematic (RTK) positioning uses the double-differenced (DD) technique to eliminate most of the systematic errors of the global navigation satellite system (GNSS) code and phase measurements. In the classical DD technique, a pivot satellite is chosen for each constellation. To obtain more of DD measurements, the mixed-constellation DD technique is proposed, forming DD measurements across different constellations. Therefore, compared with the classical technique, more high-elevation secondary satellites can be kept in the mixed-constellation DD technique. Although the mixed-constellation RTK positioning can produce more DD measurements, additional phase and code differential inter-system biases (DISBs) caused by receivers of different types and manufacturers must be estimated in the GNSS model (Odijk and Teunissen 2013; Kubo et al. 2018).

The process of resolving the integer ambiguities of the phase measurements is called ambiguity resolution (AR), and this includes the adopted model, integer ambiguity search method, and validation (Teunissen 1998). The DD ionospheric delays are one major source affecting AR performance. To facilitate AR performance, studies attempted to provide ionospheric pseudo-observations for the GNSS model. Depending on the sizes of the a priori standard deviation for the pseudo-observations, the model can be referred to as ionosphere-fixed or the ionosphere-weighting models (Odijk 2000; Odijk et al. 2000). Li et al. (2014) used a

✉ Feng-Yu Chu
fychu@nccu.edu.tw

[1] Department of Land Economics, National Chengchi University, Taipei City 116, Taiwan

[2] Tokyo University of Marine Science and Technology, Tokyo 1358533, Japan

[3] Shanghai Astronomical Observatory, Chinese Academy of Sciences, Shanghai 200030, China

Published online: 05 January 2023

bias-affected success rate proposed by Teunissen (2001) to present a formal analysis, i.e., real data are not necessary for the ionosphere-fixed and ionosphere-weighting models with levels of simulated biases. If the biases are small enough, then the AR performance with the ionosphere-fixed model can be better than that with the ionosphere-weighting model. Compared with the ionosphere-weighting model, the ionosphere-fixed model has fewer unknown parameters, contributing to better model strength. Therefore, when the biases caused by the ionospheric delays are sufficiently small, the ionosphere-fixed model can be first used to resolve the integer ambiguities. Then, the ionosphere-weighting model is used to resolve the remaining unknown parameters. This procedure is a trade-off of the two models, with which faster AR and unbiased RTK solutions can be obtained.

The Quasi-Zenith Satellite System (QZSS) is a regional space-based positioning, navigation, and timing system. The Japanese government has been developing QZSS since 2013. It presently consists of three inclined geosynchronous orbit (IGSO) satellites and one geostationary (GEO) satellite. The orbital parameters of the three IGSO satellites have specific values, which contribute to figure-8 and asymmetric ground tracks on earth and make the IGSO satellites move over the whole of Japan for a period of 8 h. Therefore, at least one IGSO satellite can be observed at elevation angles of $\geq 60°$ over the entire Japan (National Space Policy Secretariat 2020). Integrating QZSS with the other GNSS constellations can effectively improve the positioning performance of RTK positioning over the Asia–Pacific regions. Odolinski et al. (2015) used the ionosphere-fixed model to evaluate the performance improvements for short baselines. Odolinski et al. (2014) made a similar analysis with an ionosphere-weighting model for long baselines. QZSS provides three civil signals, namely L1 (1575.42 MHz), L2 (1227.60 MHz), and L5 (1176.45 MHz). The three signals are interoperable with the signals L1, L2, and L5, from GPS. Similarly, the signals L1 and L5 of QZSS are interoperable with E1 (1575.42 MHz) and E5a (1176.45 MHz) from Galileo.

Considering that the area of Japan is almost in mid-latitude regions (between 30° N and 45° N), the spatial and temporal vertical total electron content (VTEC) gradients are usually small. Related evidence has been presented by Li et al. (2020) and Cueto et al. (2012). If spatial VTEC gradients are small, when two ionospheric pierce points are close to each other, VTEC values on the two points are similar. With this condition, DD ionospheric delays formed by two high-elevation satellites can be small enough (for instance, < 10 cm) within medium-long baselines (for instance, < 200 km), because the ionospheric pierce points of the two satellites are close to each other. This finding implies that after the highest pivot satellite is chosen, if more high-elevation secondary satellites are available, then the number of DD measurements with small ionospheric delays (MSIDs) can increase. Over the entire Japan, at least one QZSS satellite can be constantly observed at high elevations of $\geq 60°$. Additionally, more high-elevation secondary satellites are available in the mixed-constellation DD technique than the classical DD technique. Therefore, the mixed-constellation DD technique that includes QZSS can make the number of DD MSIDs as large as possible in Japan. In the presence of a larger number of DD MSIDs, there is potential to obtain better AR performance. However, in general, the a priori standard deviation of the ionospheric pseudo-observations in the ionosphere-weighting model is given empirically (Odijk 2000). If the given a priori standard deviation is too large, then the small DD ionospheric delays will be estimated pessimistically. In this case, the AR performance is not effectively improved with the ionospheric pseudo-observations.

This study attempts to refine the conventional AR method of the mixed-constellation RTK positioning that includes QZSS in Japan. A cascading AR from high to low elevations is proposed to mitigate the occurrence of the problem in which the small DD ionospheric delays are pessimistically estimated. The proposed AR method is based on a trade-off between the ionosphere-fixed and the ionosphere-weighting models. Moreover, considering the use of the overlapping signals to QZSS, two constellations, namely GPS and Galileo, are adopted in this study. Although the latest BDS-3 can provide two overlapping signals to QZSS, it is not discussed. In the analysis, the conventional and the proposed AR methods are tested for positioning performance.

Evaluation of mixed-constellation DD ionospheric delays

This section discusses the size and number of mixed-constellation DD ionospheric delays. We compared the DD ionospheric delays formed by the classical and the mixed-constellation DD techniques in four cases, namely GPS-only, GPS/Galileo, GPS/Galileo/QZSS, and QZSS/GPS/Galileo, where the last case means that the pivot satellites are constantly the QZSS satellites. The IGS GIM on the first day of each month in 2019 is used to compute the DD ionospheric delays on the signal, 1575.42 MHz, that is, GPS L1. The baseline length is approximately 200 km in the middle of Japan and is formed with the stations Stn1 and Stn4, as shown in Fig. 6. The observation interval is 30 s. The satellite orbit is obtained by using the broadcast ephemeris.

Figures 1 and 2 show the RMS values and the numbers of the classical DD ionospheric delays on the 12 days (i.e., 1 January, 1 February, 1 March, and others). Figures 3 and 4 show the RMS values and the numbers of the mixed-constellation DD ionospheric delays, respectively. The elevations of the secondary satellites (ESS) are high, medium, and low when they are between 90° and 65°, 65° and 40°,

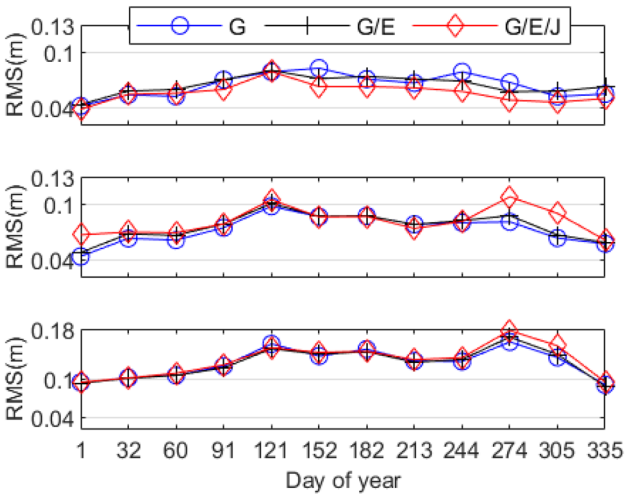

Fig. 1 RMS values of the classical DD ionospheric delays (Q: QZSS, G: GPS, E: Galileo). The top, medium, and bottom panels refer to high, medium, and low ESS, respectively

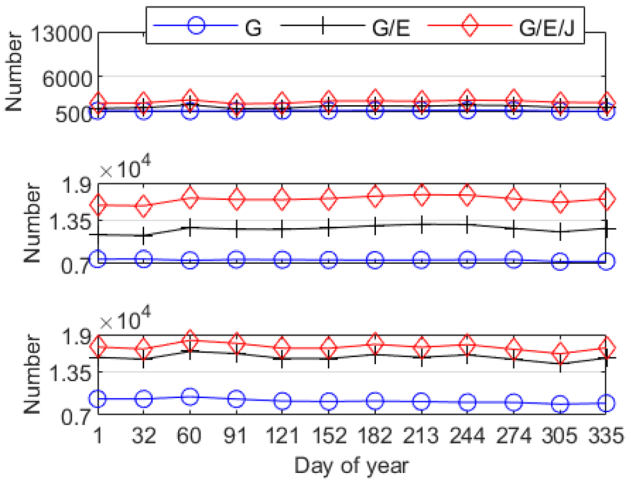

Fig. 2 Number of classical DD ionospheric delays. (Q: QZSS, G: GPS, E: Galileo). The top, medium, and bottom panels refer to high, medium, and low ESS, respectively

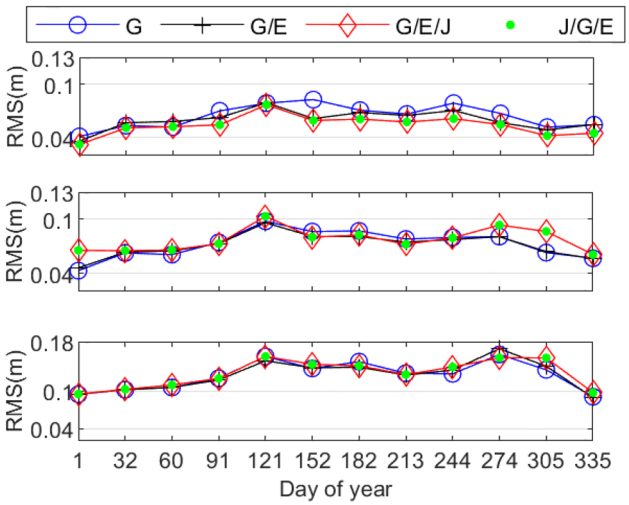

Fig. 3 RMS values of the mixed-constellation DD ionospheric delays. (Q: QZSS, G: GPS, E: Galileo). The top, medium, and bottom panels refer to high, medium, and low ESS, respectively

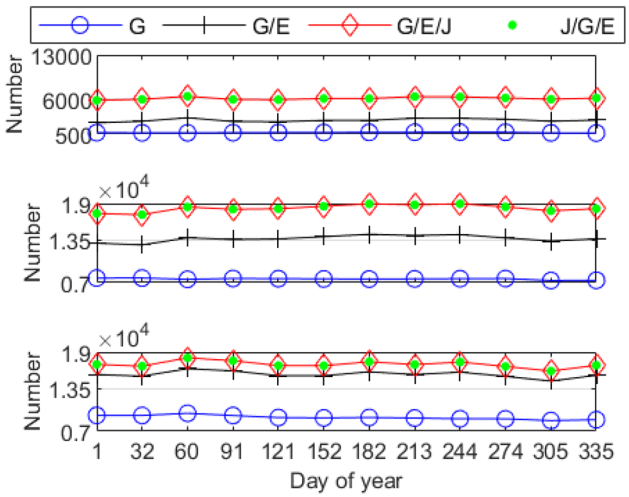

Fig. 4 Number of mixed-constellation DD ionospheric delays. (Q: QZSS, G: GPS, E: Galileo). The top, medium, and bottom panels refer to high, medium, and low ESS, respectively

and 40° and 15°, respectively. Table 1 lists the averages of the 12 days for the RMS values and the numbers when the ESS is high.

Comparisons of Figs. 1 and 3 show that the RMS values of the classical and the mixed-constellation DD ionospheric delays are similar at high ESS. The related values can be found in Table 1. From another aspect, in the comparison of Figs. 2 and 4, a significant increase can be found from the number of the classical to that of the mixed-constellation DD ionospheric delays at high ESS. The related values can be found in Table 1.

Then, for the number of mixed-constellation DD ionospheric delays, Table 1 shows that the increasing number

Table 1 Averages of 12 days for the RMS values and the number of DD ionospheric delays at high ESS

		G	*G/E*	*G/E/J*	*J/G/E*
Classical DD ion. delay	RMS (m)	0.064	0.064	0.056	
	Number	733	1343	2115	
Mixed-constellation DD ion. delay	RMS (m)	0.064	0.060	0.054	0.052
	Number	733	2681	6130	6130

from the GPS to GPS/Galileo cases is 1948 (2681–733), whereas the increasing number from the GPS/Galileo to GPS/Galileo/QZSS cases can reach 3449 (6130–2681). The latter value of 3449 is approximately two times larger than the former value of 1948, which means that using QZSS is more effective than using Galileo in increasing the number of DD ionospheric delays at high ESS. The reason is that QZSS constantly provides at least one IGSO satellite at ≥ 60° over the entire Japan.

We focus on the mixed-constellation DD ionospheric delays in the GPS/Galileo/QZSS and QZSS/GPS/Galileo cases at high ESS. Table 1 shows that the difference between the two cases is very small in RMS and zero in the number of DD ionospheric delays. The explanation is that the QZSS has the highest satellites over Japan most of the time, and they are chosen as the pivot satellites in the GPS/Galileo/QZSS case, which is almost the same as the QZSS/GPS/Galileo case.

AR methods for the mixed QZSS/GPS/Galileo RTK positioning

The above comparisons explain why QZSS is chosen as pivot satellites in the mixed-constellation DD technique most of the time in Japan, and the mixed-constellation DD technique with pivot QZSS satellites can increase the number of DD MSIDs to as large as possible. Considering the two factors, the proposed AR method is designed for the mixed-constellation DD technique with pivot QZSS satellites. In this section, the QZSS/GPS/Galileo case is used to demonstrate the proposed and conventional AR methods.

For QZSS to have two overlapping signals to all the GPS and Galileo satellites, the AR methods adopt the triple-frequency QZSS signals ($L1$, $L2$, and $L5$), the dual-frequency GPS signals ($L1$ and $L2$), and the dual-frequency Galileo signals ($E1$ and $E5a$). This study selects the dual-frequency GPS signals, namely $L1$ and $L2$, instead of $L1$ and $L5$, because all current GPS satellites are supportable for the two signals.

Mixed QZSS/GPS/Galileo measurements

Herein, mixed DD measurements and wide-lane (WL) DD measurements are described. One-way phase and code measurements can be read as follows (Teunissen and Montenbruck 2017):

$$\Phi_{r,j}^{s} = \rho_r^s + c\left(\mathrm{d}t_r - \mathrm{d}t^s\right) + c\left(\delta_{r,j}^{S} + \delta_j^s\right) + T_r^s - \mu_j^S I_r^s + \lambda_j \cdot N_{r,j}^s + \varepsilon_{r,j}^s \quad (1)$$

$$P_{r,j}^{s} = \rho_r^s + c\left(\mathrm{d}t_r - \mathrm{d}t^s\right) + c\left(d_{r,j}^{S} + d_j^s\right) + T_r^s + \mu_j^S I_r^s + e_{r,j}^s \quad (2)$$

where the subscript r identifies the receiver; the superscript S identifies the constellations; the superscript s identifies the satellites of each constellation; the subscript j refers to the signal identifier; c is the speed of light, and the symbols $\Phi_{r,j}^s$ and $P_{r,j}^s$ denote the phase and code measurements, respectively. ρ_r^s is the geometric distance; $\mathrm{d}t_r$ means the receiver clock error; $\mathrm{d}t^s$ means the satellite clock error; and $\delta_{r,j}^S$ and $d_{r,j}^S$ are the receiver phase and code biases, respectively. δ_j^s and d_j^s are the satellite phase and code biases, respectively. T_r^s means tropospheric delay; I_r^s refers to the ionospheric delay of the signal $L1$ or $E1$; $\mu_j^S = \left(F \middle/ f_j^S\right)^2$ is the ionospheric coefficient, in which the symbol f_j^S means the frequencies; and F is the frequency of signal $L1$. The $\varepsilon_{r,j}^s$ and $e_{r,j}^s$ refer to the phase and measurement noises, respectively, and they include their own multipath effects and remaining errors. The broadcast ephemeris is adopted for the satellite orbit, and the related orbital error is assumed to be neglected.

The mixed DD measurements are expressed in case the highest QZSS satellite 1_J is the pivot satellite and the two receivers are denoted as $r1$ and $r2$, as follows:

$$\Phi_{r1r2,j_{\mathrm{JJ}}}^{1_J\bar{h}} = \rho_{r1r2}^{1_J\bar{h}} + T_{r1r2}^{1_J\bar{h}} - \mu_{j_{\mathrm{JJ}}}^{J} I_{r1r2}^{1_J\bar{h}} + \lambda_{j_{\mathrm{JJ}}} \cdot N_{r1r2,j_{\mathrm{JJ}}}^{1_J\bar{h}} + \varepsilon_{r1r2,j_{\mathrm{JJ}}}^{1_J\bar{h}} \quad (3)$$

$$\Phi_{r1r2,j_{\mathrm{JG}}}^{1_Jg} = \rho_{r1r2}^{1_Jg} + c \cdot \delta_{r1r2,j_{\mathrm{JG}}}^{\mathrm{JG}} + T_{r1r2}^{1_Jg} - \mu_{j_{\mathrm{JG}}}^{J} I_{r1r2}^{1_Jg} + \lambda_{j_{\mathrm{JG}}} \cdot N_{r1r2,j_{\mathrm{JG}}}^{1_Jg} + \varepsilon_{r1r2,j_{\mathrm{JG}}}^{1_Jg} \quad (4)$$

$$\Phi_{r1r2,j_{\mathrm{JE}}}^{1_Jq} = \rho_{r1r2}^{1_Jq} + c \cdot \delta_{r1r2,j_{\mathrm{JE}}}^{\mathrm{JE}} + T_{r1r2}^{1_Jq} - \mu_{j_{\mathrm{JE}}}^{J} I_{r1r2}^{1_Jq} + \lambda_{j_{\mathrm{JE}}} \cdot N_{r1r2,j_{\mathrm{JE}}}^{1_Jq} + \varepsilon_{r1r2,j_{\mathrm{JE}}}^{1_Jq} \quad (5)$$

$$P_{r1r2,j_{\mathrm{JJ}}}^{1_J\bar{h}} = \rho_{r1r2}^{1_J\bar{h}} + T_{r1r2}^{1_J\bar{h}} + \mu_{j_{\mathrm{JJ}}}^{J} I_{r1r2}^{1_J\bar{h}} + e_{r1r2,j_{\mathrm{JJ}}}^{1_J\bar{h}} \quad (6)$$

$$P_{r1r2,j_{\mathrm{JG}}}^{1_Jg} = \rho_{r1r2}^{1_Jg} + c \cdot d_{r1r2,j_{\mathrm{JG}}}^{\mathrm{JG}} + T_{r1r2}^{1_Jg} + \mu_{j_{\mathrm{JG}}}^{J} I_{r1r2}^{1_Jg} + e_{r1r2,j_{\mathrm{JG}}}^{1_Jg} \quad (7)$$

$$P_{r1r2,j_{\mathrm{JE}}}^{1_Jq} = \rho_{r1r2}^{1_Jq} + c \cdot d_{r1r2,j_{\mathrm{JE}}}^{\mathrm{JE}} + T_{r1r2}^{1_Jq} + \mu_{j_{\mathrm{JE}}}^{J} I_{r1r2}^{1_Jq} + e_{r1r2,j_{\mathrm{JE}}}^{1_Jq} \quad (8)$$

where the satellites for QZSS, GPS, and Galileo are denoted as $\bar{h}$, g, and q, respectively; $\bar{h} = 2_J, \cdots, m_J$, $g = 1_G, \cdots, m_G$, and $q = 1_E, \cdots, m_E$; m_J, m_G, and m_E refer to the number of satellites; the subscript $j_{\mathrm{JJ}} = L1, L2, L5$; the subscript $j_{\mathrm{JG}} = L1, L2$; and the subscript $j_{\mathrm{JE}} = L1$ (i.e., $E1$), $L5$ (i.e., $E5a$). The symbols $\delta_{r1r2,j}^{\mathrm{JG}}$ and $d_{r1r2,j}^{\mathrm{JG}}$ mean the QZSS-GPS phase and code DISBs, respectively. The $\delta_{r1r2,j}^{\mathrm{JE}}$ and $d_{r1r2,j}^{\mathrm{JE}}$ mean the QZSS-Galileo phase and code DISBs, respectively.

The WL linear combinations are widely used to improve AR performance, because its long wavelengths are effective

against the influence of systematic errors (Chu et al. 2016). The mixed DD WL linear combinations are expressed as follows:

$$\Phi^{1_J\bar{h}}_{r1r2,\mathrm{WL}_{L1/L2}} = \rho^{1_J\bar{h}}_{r1r2} + \lambda_{\mathrm{WL}_{L1/L2}} \cdot N^{1_J\bar{h}}_{r1r2,\mathrm{WL}_{L1/L2}} + \varepsilon^{1_J\bar{h}}_{r1r2,\mathrm{WL}_{L1/L2}} \tag{9}$$

$$\Phi^{1_J\bar{h}}_{r1r2,\mathrm{WL}_{L1/L5}} = \rho^{1_J\bar{h}}_{r1r2} + \lambda_{\mathrm{WL}_{L1/L5}} \cdot N^{1_J\bar{h}}_{r1r2,\mathrm{WL}_{L1/L5}} + \varepsilon^{1_J\bar{h}}_{r1r2,\mathrm{WL}_{L1/L5}} \tag{10}$$

$$\Phi^{1_Jg}_{r1r2,\mathrm{WL}_{L1/L2}} = \rho^{1_Jg}_{r1r2} + c \cdot \delta^{\mathrm{JG}}_{r1r2,\mathrm{WL}_{L1/L2}} + \lambda_{\mathrm{WL}_{L1/L2}} \cdot N^{1_Jg}_{r1r2,\mathrm{WL}_{L1/L2}} + \varepsilon^{1_Jg}_{r1r2,\mathrm{WL}_{L1/L2}} \tag{11}$$

$$\Phi^{1_Jq}_{r1r2,\mathrm{WL}_{L1/L5}} = \rho^{1_Jq}_{r1r2} + c \cdot \delta^{\mathrm{JE}}_{r1r2,\mathrm{WL}_{L1/L5}} + \lambda_{\mathrm{WL}_{L1/L5}} \cdot N^{1_Jq}_{r1r2,\mathrm{WL}_{L1/L5}} + \varepsilon^{1_Jq}_{r1r2,\mathrm{WL}_{L1/L5}} \tag{12}$$

$$P^{1_J\bar{h}}_{r1r2,\mathrm{WL}_{L1/L2}} = \rho^{1_J\bar{h}}_{r1r2} + e^{1_J\bar{h}}_{r1r2,\mathrm{WL}_{L1/L2}} \tag{13}$$

$$P^{1_J\bar{h}}_{r1r2,\mathrm{WL}_{L1/L5}} = \rho^{1_J\bar{h}}_{r1r2} + e^{1_J\bar{h}}_{r1r2,\mathrm{WL}_{L1/L5}} \tag{14}$$

$$P^{1_Jg}_{r1r2,\mathrm{WL}_{L1/L2}} = \rho^{1_Jg}_{r1r2} + c \cdot d^{\mathrm{JG}}_{r1r2,\mathrm{WL}_{L1/L2}} + e^{1_Jg}_{r1r2,\mathrm{WL}_{L1/L2}} \tag{15}$$

$$P^{1_Jq}_{r1r2,\mathrm{WL}_{L1/L5}} = \rho^{1_Jq}_{r1r2} + c \cdot d^{\mathrm{JE}}_{r1r2,\mathrm{WL}_{L1/L5}} + e^{1_Jq}_{r1r2,\mathrm{WL}_{L1/+L5}} \tag{16}$$

where the influence of the ionospheric and tropospheric delays is assumed to be negligible, but when the baseline is too long (for instance, > 200 km), this assumption cannot hold true.

Conventional AR method

The conventional AR method includes two steps. The first step is to resolve the integer WL ambiguities, and the second step is to resolve the phase ambiguities. In the first step, the linearized observation equations are expressed as follows:

$$\begin{cases} E(\mathbf{y}_{\mathrm{WL}}) = \mathbf{A}_1 \cdot \mathbf{a}_{\mathrm{WL}} + \mathbf{B}_1 \cdot \mathbf{b} + \mathbf{C}_1 \cdot \mathbf{c}_{\mathrm{WL}},\ D(\mathbf{y}_{\mathrm{WL}}) = \mathrm{Q}_{\mathbf{y}_{\mathrm{WL}}\mathbf{y}_{\mathrm{WL}}} \\ \tilde{N}^{1_J1_G}_{r1r2,\mathrm{WL}_{L1/L2}} = \mathbf{H}_1 \cdot \mathbf{a}_{\mathrm{WL}} \\ \tilde{N}^{1_J1_E}_{r1r2,\mathrm{WL}_{L1/L5}} = \mathbf{H}_2 \cdot \mathbf{a}_{\mathrm{WL}} \end{cases} \tag{17}$$

where the symbol $E(.)$ refers to the expectation value, and the symbol $D(.)$ refers to the dispersion operator. The observation vector $\mathbf{y}_{\mathrm{WL}}$ comprises the WL linear combinations minus the computed values. The parameter vector $\mathbf{a}_{\mathrm{WL}}$ comprises the WL ambiguities and is expressed as follows:

$$\mathbf{a}_{\mathrm{WL}} = \underset{1\times(2\cdot m_J+m_G+m_E-2)}{\left[N^{1_J\bar{h}}_{r1r2,\mathrm{WL}_{L1/L2}} \quad N^{1_J\bar{h}}_{r1r2,\mathrm{WL}_{L1/L5}} \quad N^{1_Jg}_{r1r2,\mathrm{WL}_{L1/L2}} \quad N^{1_Jg}_{r1r2,\mathrm{WL}_{L1/L5}} \right]^T} \tag{18}$$

The parameter vector $\mathbf{b}$ includes three baseline components. The parameter vector $\mathbf{c}_{\mathrm{WL}}$ includes the DISBs and is expressed as follows:

$$\mathbf{c}_{\mathrm{WL}} = \left[\delta^{\mathrm{JG}}_{r1r2,\mathrm{WL}_{L1/L2}} \quad \delta^{\mathrm{JE}}_{r1r2,\mathrm{WL}_{L1/L5}} \quad d^{\mathrm{JG}}_{r1r2,\mathrm{WL}_{L1/L2}} \quad d^{\mathrm{JE}}_{r1r2,\mathrm{WL}_{L1/L5}} \right]^T \tag{19}$$

The symbols $\mathbf{A}_1$, $\mathbf{B}_1$, $\mathbf{C}_1$, and $\mathbf{H}_1$ identify the design matrices. The symbol $\tilde{N}^{1_J1_G}_{r1r2,\mathrm{WL}_{L1/L2}}$ is an arbitrarily given integer value for the WL DD ambiguity formed by the pivot QZSS satellite 1_J and GPS satellite 1_G. Similarly, $\tilde{N}^{1_J1_E}_{r1r2,\mathrm{WL}_{L1/L5}}$ is a given integer value for the WL DD ambiguity formed by the satellite 1_J and Galileo satellite 1_E. The two integer values $\tilde{N}^{1_J1_G}_{r1r2,\mathrm{WL}_{L1/L2}}$ and $\tilde{N}^{1_J1_E}_{r1r2,\mathrm{WL}_{L1/L5}}$ are treated as constraints in (17). If the constraints are absent, then estimating the DISBs and ambiguities simultaneously cannot be achieved because of rank deficiency.

The unknown parameters of (17) are estimated by the Kalman filter (Strang and Borre 1997), where the transition matrix is given with an identity matrix, and the process noises are normally distributed with a zero mean. The standard deviations for the process noises are given in Table 2. To recover the integer property, the LAMBDA method (Teunissen 1995) is used to obtain the integer ambituses $\breve{\mathbf{a}}_{\mathrm{WL}}$. Moreover, the success rate and the ratio test are used for ambiguity validation. The threshold of the test is given

Table 2 Information for the process noises of the Kalman filter

Parameter	Standard deviation	Description
Baseline components	$\pm\infty$ (m)	Kinematic solutions
Ambiguities	± 0 (m)	Constants
DISBs	± 0 (m)	Constants
DD ion. delays	$\pm 0.03 \Big/ \sqrt{\mathrm{sec}}$ (m)	A commonly used value
RZTD	$\pm 0.0003 \Big/ \sqrt{\mathrm{sec}}$ (m)	A commonly used value

with a commonly used value of 2 (Teunissen and Verhagen 2009).

After the LAMBDA method, the resolved integer WL ambiguities $\breve{\mathbf{a}}_{\mathrm{WL}}$ are introduced as constraints into the second step. The linearized observations of the second step are expressed as follows:

$$\begin{cases} E(\mathbf{y}) = \mathbf{A}_2 \cdot \mathbf{a} + \mathbf{B}_1 \cdot \mathbf{b} + \mathbf{C}_2 \cdot \mathbf{c} + \mathbf{D} \cdot \mathbf{d} + \mathbf{M} \cdot \mathrm{RZTD},\ D(\mathbf{y}) = \mathbf{Q}_{\mathbf{yy}} \\ \breve{\mathbf{a}}_{\mathrm{WL}} = \mathbf{H}_3 \cdot \mathbf{a} \\ \mathbf{y}_{\tilde{N}} = \mathbf{H}_4 \cdot \mathbf{a} \end{cases} \tag{20}$$

where the observation vector $\mathbf{y}$ includes the DD measurements by (3)–(8), in which the related computed values have been removed. The residual values of the tropospheric delays are absorbed with the relative zenith tropospheric delay (RZTD) parameter. The observation vector $\mathbf{y}_{\tilde{N}}$ includes arbitrarily given integer values for the QZSS-GPS and QZSS-Galileo DD ambiguities, which are expressed as follows:

$$\mathbf{y}_{\tilde{N}} = [\, \tilde{N}^{1_J 1_G}_{r1r2,j_{\mathrm{JG}}} \ \tilde{N}^{1_J 1_E}_{r1r2,j_{\mathrm{JE}}} \,]_{1\times 4} \tag{21}$$

The parameter vector $\mathbf{a}$ includes the following ambiguities:

$$\mathbf{a} = \left[N^{1_J \bar{h}}_{r1r2,j_{\mathrm{JJ}}} \ N^{1_J g}_{r1r2,j_{\mathrm{JG}}} \ N^{1_J q}_{r1r2,j_{\mathrm{JE}}} \right]^T_{1\times(3\cdot m_J + 2\cdot m_G + 2\cdot m_E - 3)} \tag{22}$$

The parameter vector $\mathbf{c}$ includes DISBs and is expressed as follows:

$$\mathbf{c} = \left[\delta^{\mathrm{JG}}_{r1r2,j_{\mathrm{JG}}} \ \delta^{\mathrm{JE}}_{r1r2,j_{\mathrm{JE}}} \ d^{\mathrm{JG}}_{r1r2,j_{\mathrm{JG}}} \ d^{\mathrm{JE}}_{r1r2,j_{\mathrm{JE}}} \right]^T_{1\times 8} \tag{23}$$

The parameter vector $\mathbf{d}$ identifies the DD ionospheric delays and is expressed as follows:

$$\mathbf{d} = \left[I^{1_J \bar{h}}_{r1r2} \ I^{1_J g}_{r1r2} \ I^{1_J q}_{r1r2} \right]^T_{1\times(m_J + m_G + m_E - 1)} \tag{24}$$

The symbols $\mathbf{A}_2$, $\mathbf{C}$, $\mathbf{D}$, $\mathbf{M}$, $\mathbf{H}_3$, and $\mathbf{H}_4$ identify their corresponding designed matrices.

To facilitate the AR performance, additional pseudo-observations for the DD ionospheric delays and RZTD are usually incorporated with (20). The pseudo-observations of the RZTD, denoted as RZTD_0, are expressed as follows:

$$E(\mathrm{RZTD}_0) = 0,\ D(\mathrm{RZTD}_0) = \sigma^2_{\mathrm{RZTD}_0} \tag{25}$$

where σ_{RZTD_0} means the a priori standard deviation of the parameter RZTD. Then, the pseudo-observations for the DD ionospheric delays, denoted as the vector $\mathbf{I}_0$, are expressed as follows:

$$E(\mathbf{I}_0) = 0,\ D(\mathbf{I}_0) = Q_{\mathbf{I}_0\mathbf{I}_0} = \sigma^2_{I_0} \cdot \mathbf{e}_{(m_J + m_G + m_E - 1)\times(m_J + m_G + m_E - 1)} \tag{26}$$

where the matrix e is an identity matrix, and σ_{I_0} is the a priori standard deviation of the DD ionospheric delays. When the standard deviation σ_{I_0} is zero, equation (20) is the ionosphere-fixed model. When the standard deviation σ_{I_0} is not zero, equation (20) is called the ionosphere-weighting model (Odijk et al. 2000). We also neglected the influence of the tropospheric delays, that is, $\sigma_{\mathrm{RZTD}_0} = 0$, in the ionosphere-fixed model to further improve its strength and give $\sigma_{\mathrm{RZTD}_0} = 10$ cm in the ionosphere-weighting model.

The conventional AR method theoretically performs in an equivalent manner to AR methods based on the classical DD measurements. The mixed-constellation DD technique produces additional DD measurements in contrast to the classical DD technique, but the DISBs are present in the mixed-constellation DD measurements. Thus, the additional DD measurements contribute nothing to the AR performance (Odijk and Teunissen 2013).

Proposed AR method

From (26), the a priori standard deviation is the same and given empirically for all the ionospheric pseudo-observations. The a priori standard deviation is regularly given a value large enough for the largest DD ionospheric delay. However, if DD ionospheric delays formed at high elevations are relatively small, they will be pessimistically estimated. In this case, the AR performance will not be effectively improved. Therefore, the proposed AR method aims to mitigate the occurrence of the problem.

The proposed AR method adopts a trade-off of the ionosphere-fixed and ionosphere-weighting models. Conceptually, the proposed AR method first resolves a subset of integer ambiguities with the ionosphere-fixed model. The subset comprises the integer ambiguities of DD measurements affected by small ionospheric delays. Then, the resolved subset of integer ambiguities, denoted as $\breve{\mathbf{a}}_{\mathrm{sub}}$, is introduced into the ionosphere-weighting model as a constraint to estimate the remaining parameters. The observation equations can be expressed as follows:

$$\begin{cases} E(\mathbf{y}) = \mathbf{A}_2 \cdot \mathbf{a} + \mathbf{B}_1 \cdot \mathbf{b} + \mathbf{C}_2 \cdot \mathbf{c} + \mathbf{D} \cdot \mathbf{d} + \mathbf{M} \cdot \mathrm{RZTD},\ D(\mathbf{y}) = \mathbf{Q}_{\mathbf{yy}} \\ \breve{\mathbf{a}}_{\mathrm{WL}} = \mathbf{H}_3 \cdot \mathbf{a} \\ \mathbf{y}_{\tilde{N}} = \mathbf{H}_4 \cdot \mathbf{a} \\ \breve{\mathbf{a}}_{\mathrm{sub}} = \mathbf{H}_5 \cdot \mathbf{a} \end{cases} \tag{27}$$

where $\mathbf{H}_5$ identifies the design matrix of $\breve{\mathbf{a}}_{\mathrm{sub}}$. Different from the trade-off in Li et al. (2014) that resolves all integer ambiguities with the ionosphere-fixed model, the proposed AR method only uses the ionosphere-fixed model to resolve $\mathbf{a}_{\mathrm{sub}}$. Moreover, compared with the trade-off in Chu et al. (2019), a different strategy is used to determine the subset $\breve{\mathbf{a}}_{\mathrm{sub}}$.

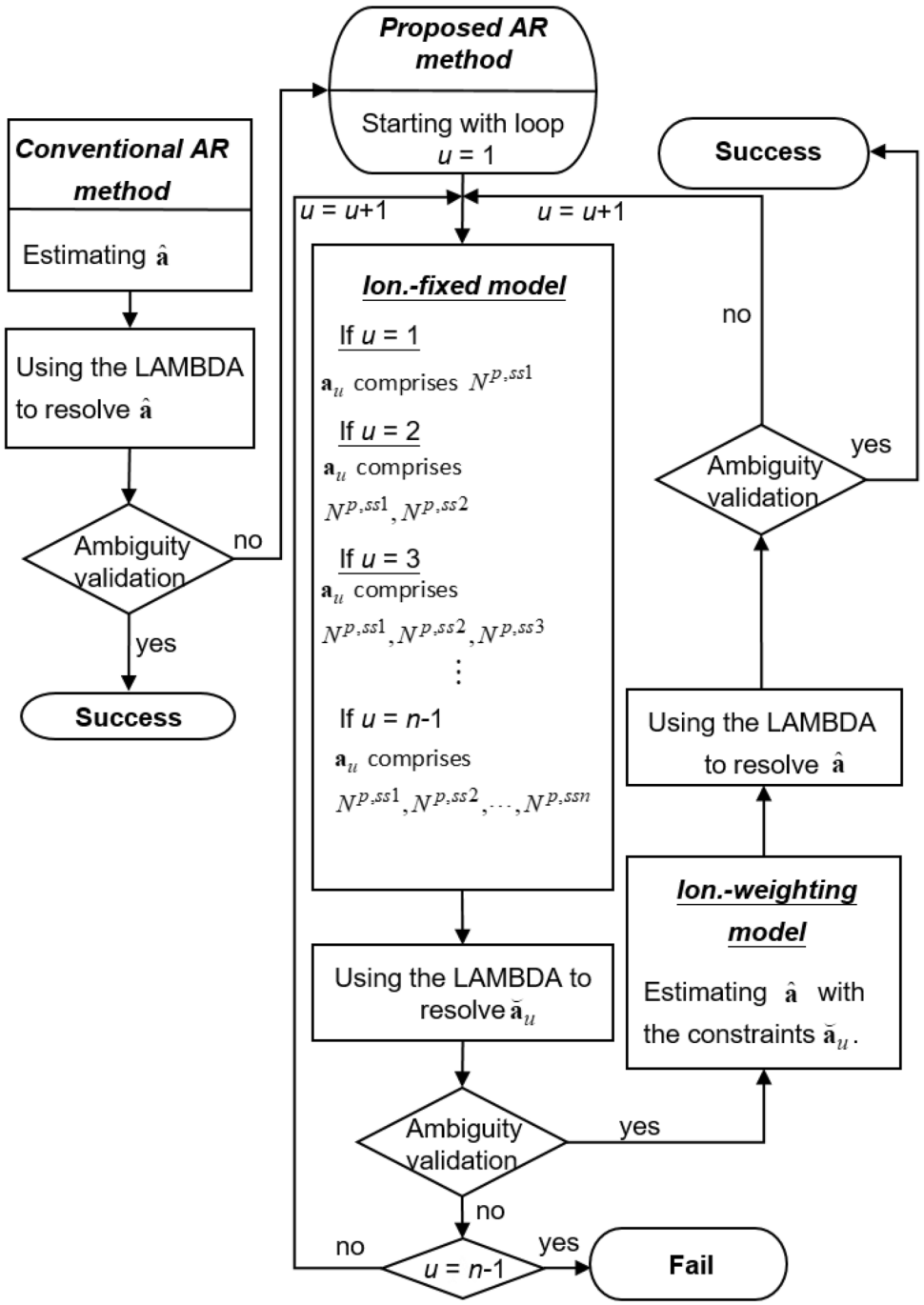

Fig. 5 Flowchart of the proposed AR method. The method is implemented with several loops. The symbol u indicates the order of the loops

When the conventional AR method cannot produce confident integer ambiguities, the proposed AR is triggered. The detailed procedure is implemented with several loops, as shown in Fig. 5, in which n satellites are assumed. In the first loop, we assume that the DD measurements formed with the highest secondary satellite are affected by small ionospheric delays. The secondary satellite is denoted as $ss1$, and the DD ambiguity is denoted as $N^{p,ss1}$, where the symbol p refers to the pivot satellite. A subset $\mathbf{a}_1$ comprises the integer DD ambiguity, and then, the ionosphere-fixed models are used to resolve the integer ambiguity. When the success rate is $\geq 95\%$, and the ratio test value is ≥ 2, the resolved subset $\breve{\mathbf{a}}_1$ can pass the ambiguity validation and then be treated as $\breve{\mathbf{a}}_{\text{sub}}$ in (27) to resolve all the integer ambiguities in $\mathbf{a}$. If the resolved $\breve{\mathbf{a}}$ also passes the ambiguity validation, then the procedure ends and achieves the AR. Otherwise, the second loop is necessary. In the second loop, we additionally assume that the DD measurement formed by the second highest secondary satellite, denoted as $ss2$, is affected by small ionospheric delays. Then, the ionosphere-fixed model

is again used to resolve a subset $\mathbf{a}_2$, including the previous $N^{p,ss1}$ and $N^{p,ss2}$. If the resolved $\breve{\mathbf{a}}_2$ passes the ambiguity validation, then the subset is similarly treated as $\breve{\mathbf{a}}_{\text{sub}}$ in (27) to resolve $\mathbf{a}$. The procedure continues until total n satellites have been used.

Experiment and analysis

The performance of the RTK positioning, including the AR performance and the positioning accuracy, is evaluated here. Three test baselines located in the middle of Japan are collected with receivers Trimble NetR9 from the Geospatial Information Authority of Japan on March 1, 2019. Figure 6 shows the geographic distributions of the three test baselines, and their lengths are 10, 100, and 200 km. The observation period is 1 day (24 h), and the observation interval is 30 s. Figure 7 shows the DD ionospheric delays at different ESS. The figure shows that the DD ionospheric delays increase when the baseline length increases, and they decrease when the ESS ascends. During the process of the three test baselines, the elevation cutoff angle is 15°.

Figure 8 shows the estimated phase DISBs (the integer part has been removed) and code DISBs on each frequency with the conventional AR method for the QZSS/GPS/Galileo case. The σ_{I_0} is given with ∞ in the ionosphere-weighting model, meaning ionospheric pseudo-observations are not used in the mode. These DISBs are estimable, and the values are stable. The results are reasonable in accordance with Odijk and Teunissen (2013) and Mi et al. (2019).

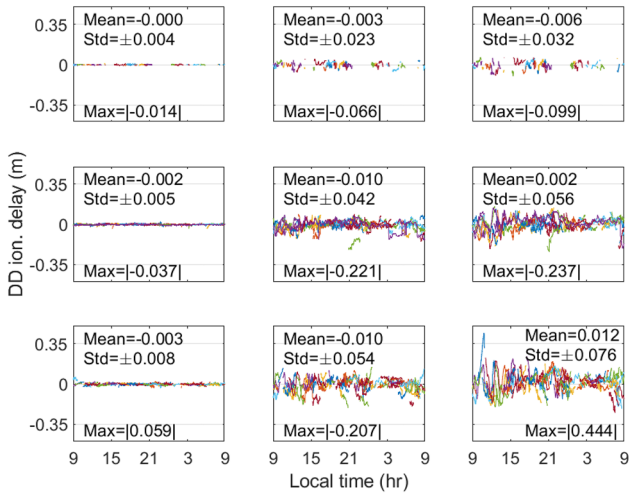

Fig. 7 DD ionospheric delays and the related statistic values for the three test baselines. The top, medium, and bottom rows refer to the cases with high, medium, and low ESS, respectively. The left, medium, and right columns refer to the baselines 10, 100, and 200 km, respectively

AR performance

The success percentage is defined to quantify the AR performance, as follows:

$$\text{Success percentage} = \frac{N_{\text{correct}}}{48} \times 100\% \tag{28}$$

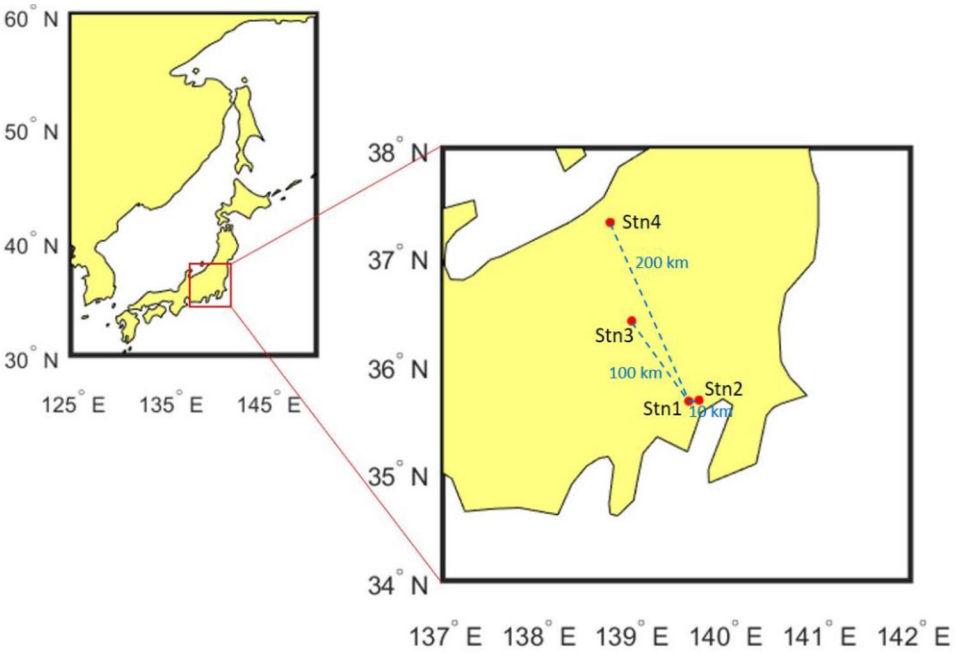

Fig. 6 Geographic distribution of the test baselines

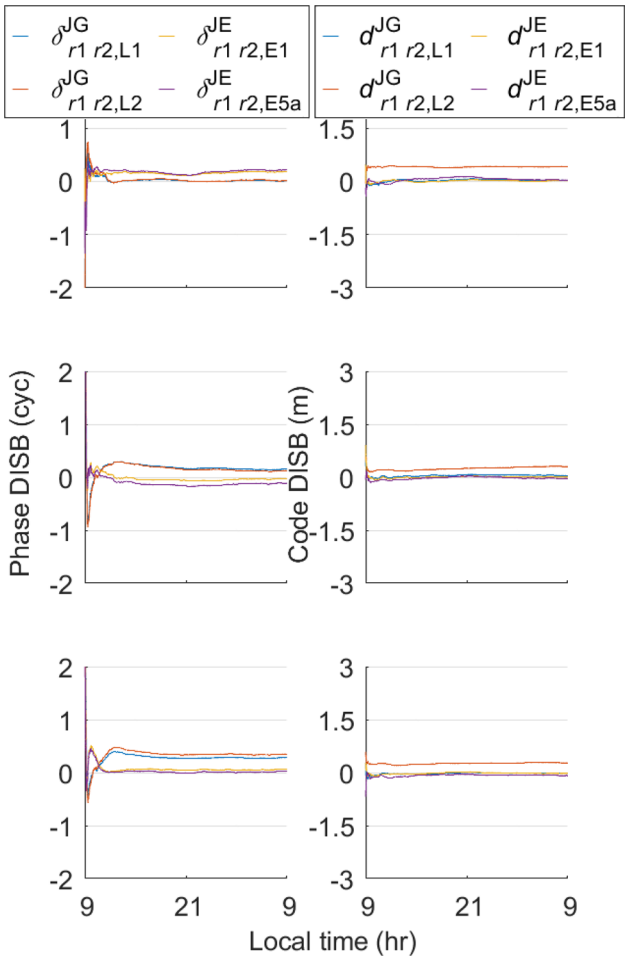

Fig. 8 Estimated DISBs. The top, medium, and bottom panels are the results of the 10, 100, and 200 km baselines, respectively

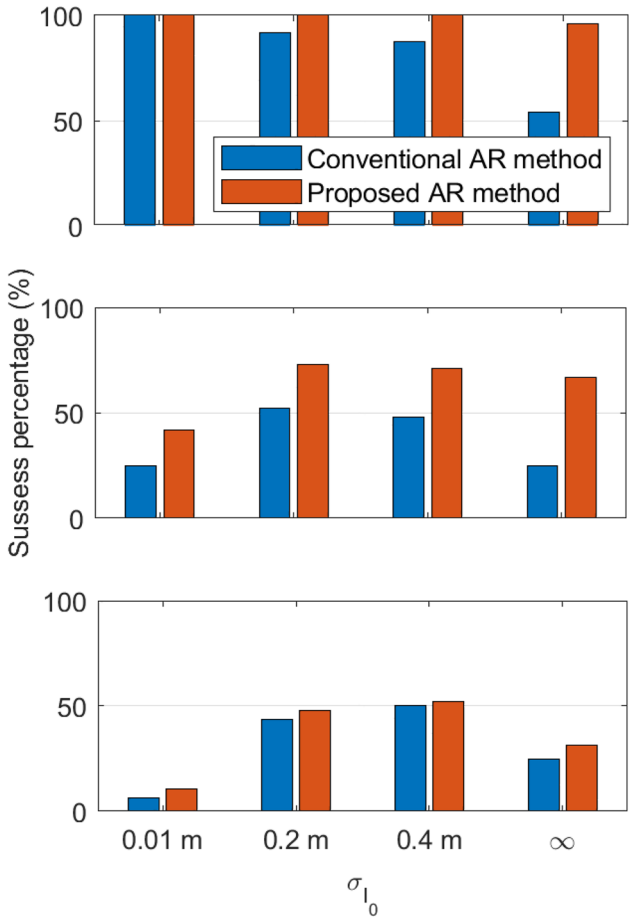

Fig. 9 Success percentage of the conventional and proposed AR methods for the QZSS/GPS/Galileo case. The top, medium, and bottom panels are the results of the 10, 100, and 200 km baselines, respectively

The 24 h observation span is initialized every 30 min, and hence, a total of 48 test sessions were used in the success percentage. Considering that the test baselines are formed with static stations, the reference values of the integer ambiguities of each test session are computed with a static process. If a test session can pass the ambiguity validation within 5 min, and the integer ambiguities are correctly resolved, then the test session is deemed successful. The total number of successful sessions is denoted as N_{correct}.

The success percentage of the conventional and proposed AR methods is computed with four conditions, as follows: $\sigma_{I_0} = 0.01$, 0.2, 0.4, ∞m. Figures 9 and 10 depict the results of the QZSS/GPS/Galileo and QZSS/GPS cases, respectively. In the QZSS/GPS/Galileo case, for the 10 km baseline, the success percentage is 100% for the conventional and proposed AR methods at $\sigma_{I_0} = 0.01$ m. The reason is that all the DD ionospheric delays over the baseline are small enough. Moreover, both methods have sufficient model strength to achieve a confident success percentage at $\sigma_{I_0} = 0.01$ m. When σ_{I_0} becomes large, the success percentage of the conventional AR method decreases evidently, because the model strength decreases. By contrast, the proposed AR method can still provide approximately 96% success percentage even at $\sigma_{I_0} = \infty$.

The results of the 100 km baseline showed that the proposed AR method is superior to the conventional AR method under all four conditions of σ_{I_0}. The minimum improvement occurs at $\sigma_{I_0} = 0.01$ m, because σ_{I_0} is given optimistically for the test baseline, leading to a low success percentage for the two methods. The maximum improvement is 41.7% (66.7% − 25%), which occurs at $\sigma_{I_0} = \infty$, because the model strength of the conventional AR method is the weakest, whereas that of the proposed AR method is refined with the trade-off. The results of the 200 km baseline indicate that small improvements are produced by the proposed AR method. The maximum improvement is only 6.3% (31.3% − 25%), which occurs at $\sigma_{I_0} = \infty$. Most of the DD

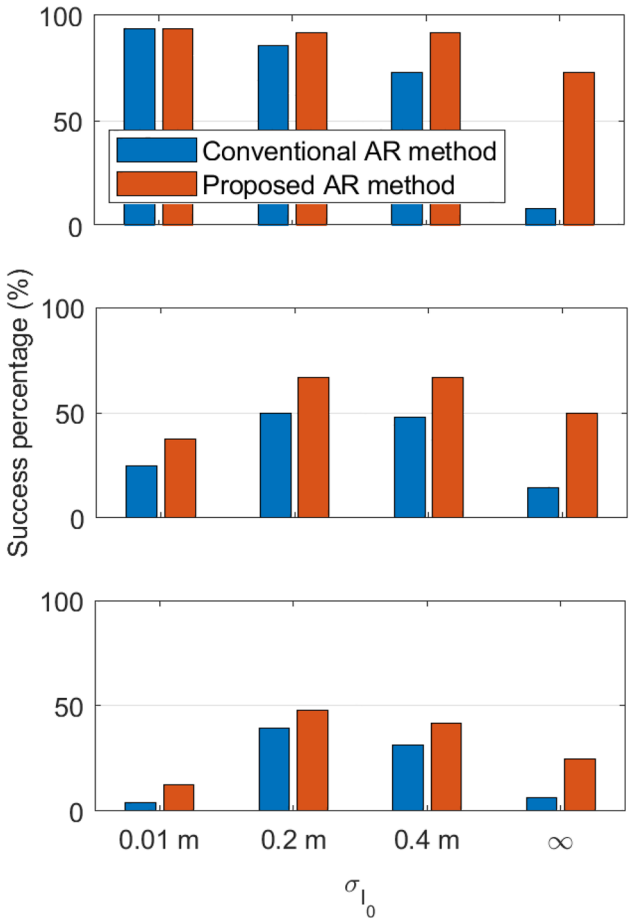

Fig. 10 Success percentage of the conventional and proposed AR methods for the QZSS/GPS case. The top, medium, and bottom panels are the results of the 10, 100, and 200 km baselines, respectively

ionospheric delays are not small enough for the baseline. Thus, the trade-off cannot effectively refine the model strength.

The proposed AR method can perform as satisfactorily as the conventional AR method when the influence of the DD ionospheric delay is small enough, for example, short baselines of < 10 km. However, when the influence of the DD ionospheric delays becomes large, the conventional and proposed AR methods perform down, but the proposed AR method has better resistance to such influence.

Similar to the results of the QZSS/GPS/Galileo case, Fig. 10 shows that the proposed AR method has better resistance to ionospheric delays than the conventional AR method in the QZSS/GPS case. However, comparing Figs. 9 and 10 shows that the QZSS/GPS/Galileo case performs better than the QZSS/GPS case. The reason is that the QZSS/GPS /Galileo case provides better satellite geometry than the QZSS/GPS case.

Positioning accuracy analysis

In this section, we focus on the impact of AR on the positioning accuracy. The above section indicates that the proposed AR method performs better than the conventional AR method in both the QZSS/GPS/Galileo and QZSS/GPS cases. Therefore, in this analysis, we only demonstrate the positioning accuracy with the QZSS/GPS/Galileo case. The positioning accuracy for the 48 sessions of the three test baselines is discussed. Three kinds of positioning solutions are used in this analysis. When all integer ambiguities can be confidently resolved, the result is called a full-fixing AR (FAR) solution. In case resolving all integer ambiguities cannot be confidently achieved, we try to resolve a subset of confident integer ambiguities to refine the positioning accuracy, and this is the so-called partial-fixing AR (PAR) solution. Verhagen and Li (2012) presented a detailed theory of the PAR solution and the related process. If no confident integer ambiguities can be obtained, then it is treated as a float solution.

As shown in Fig. 5, the proposed AR method is only designed to achieve the FAR solution. Therefore, when the FAR solution is unavailable, the proposed AR method provides either the float or PAR solution. The proposed and conventional AR methods provide the same solutions in this situation. The PAR solution has to reach a ratio test value of ≥ 2 in this analysis. Otherwise, the float solution will be adopted. The reference coordinates are computed by using a static process, in which the entire 24 h observation period is used. Moreover, RMS values and FAR rates are used to evaluate the results. The RMS values are computed with three-dimensional positioning errors (TDPE) collected from the 10 epochs to 60 epochs of every session (i.e., after a 5-min initialization in every session), which can be expressed as follows:

$$\mathrm{RMS} = \sqrt{\frac{\sum_{K=1}^{48}\left(\sum_{\mathrm{epoch}=10}^{60}\mathrm{TDPE}_{\mathrm{epoch}}^{2}\right)_K}{51\times 48}} \tag{29}$$

where K is the session number. The FAR rate means the percentage of the number of epochs achieving the FAR solutions in the entire 24 h observation period.

Figure 11 shows the positioning results of the 10 km baseline. Compared with the conventional AR method, the proposed AR method does not have evident improvements in positioning accuracy when a sufficiently small σ_{I_0} is given, mainly because most of the DD ionospheric delays are small enough. On the contrary, under the last condition, $\sigma_{I_0} = \infty$ m, the FAR rate of the proposed AR method is evidently larger than that of the conventional AR method. Thus, the proposed

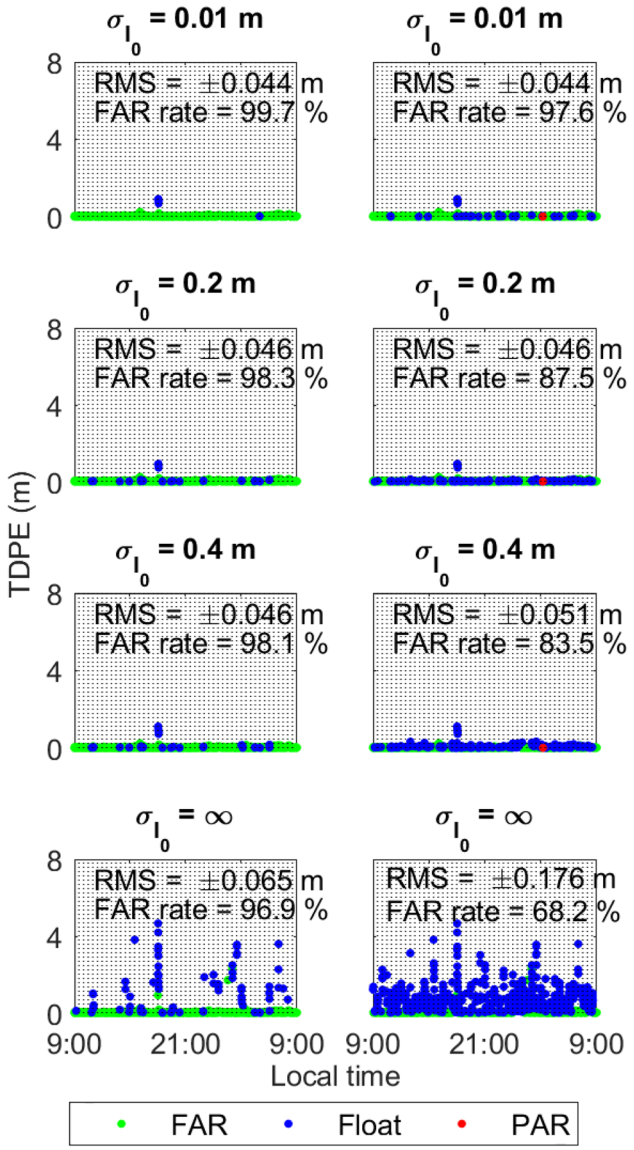

Fig. 11 Positioning errors of the 10 km baseline. The left and right columns refer to the proposed and conventional AR methods, respectively

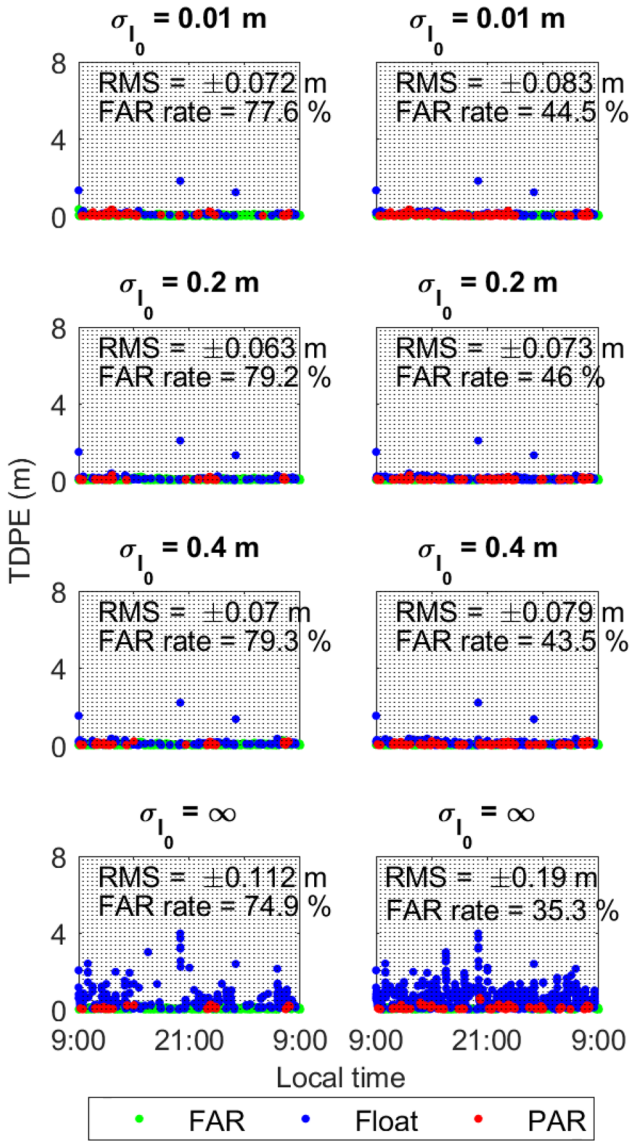

Fig. 12 Positioning errors of the 100 km baseline. The left and right columns refer to the proposed and conventional AR methods, respectively

AR method is significantly better than the conventional AR method in positioning accuracy under this condition.

Figure 12 shows the positioning results of the 100 km baseline, where the FAR rates of the proposed AR method under the four conditions of σ_{I_0} are evidently larger than those of the conventional AR method. Thus, the proposed AR method significantly performs better than the conventional AR method in terms of positioning accuracy. The maximum improvement of the RMS values can reach 41.1% ($(0.19-0.112)/0.19\times100$), under the condition of $\sigma_{I_0}=\infty$.

As shown in Fig. 13, in contrast to the conventional AR method, the proposed AR method improves small in positioning accuracy for the 200 km baseline at all four conditions, because the FAR rates of the proposed AR method are not substantially higher than those of the conventional AR method. The maximum improvement of the RMS values occurs at $\sigma_{I_0}=\infty$ m, but it can only reach 7.8% ($(0.179-0.165)/0.179\times100$).

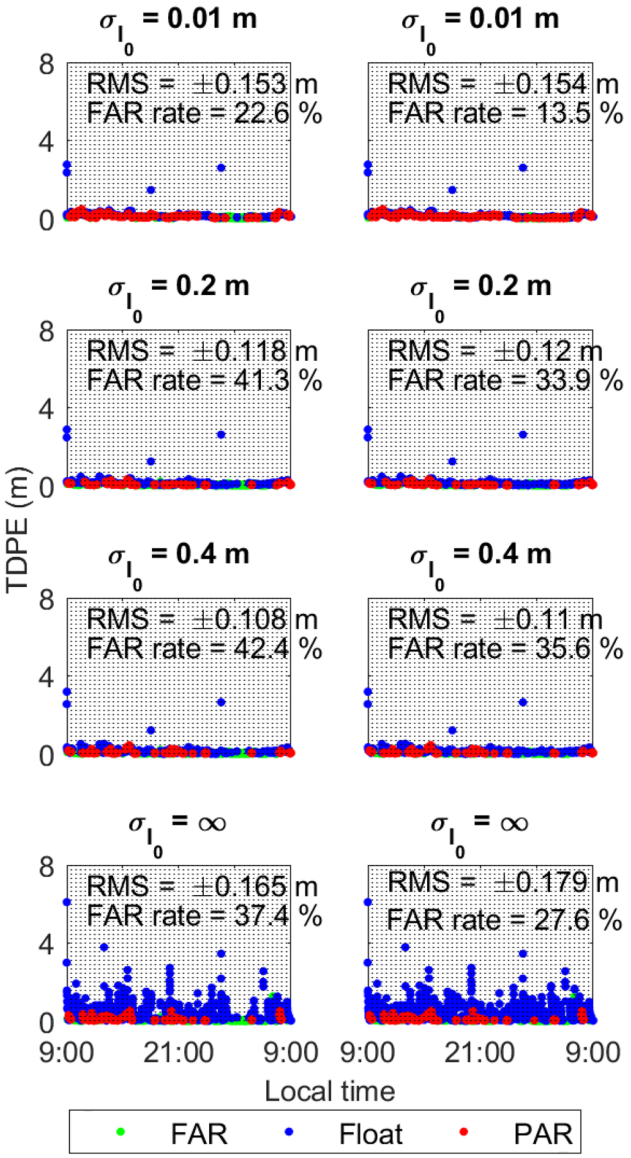

Fig. 13 Positioning errors of the 200 km baseline. The left and right columns refer to the proposed and conventional AR methods, respectively

Conclusions

This study proposes a cascading AR from high to low elevations to refine the mixed QZSS/GPS/Galileo RTK positioning in Japan. Two issues are discussed. In the first issue, the size and number of DD ionospheric delays in the middle of Japan are investigated. The mixed-constellation DD technique with pivot QZSS satellites enables the number of DD MSIDs to be as large as possible in Japan. Then, the proposed AR method is designed with pivot QZSS satellites in the second issue.

The proposed AR method adopts a trade-off between the ionosphere-fixed and ionosphere-weighting models to resolve the inter ambiguities. Compared with the conventional AR method, the experimental results show that the proposed AR method is similarly affected by the influence of the ionospheric delays but has better resistibility to the influence. The experimental results also show that the proposed AR method can improve the AR performance and the positioning accuracy for medium-long baselines. The success percentage of AR can improve by 41.7% and 6.5% for the 100 and 200 km test baselines, respectively. The improvements of the positioning accuracy can reach 41.1% and 7.8% in RMS for the 100 and 200 km test baselines, respectively.

Presently, the proposed AR method is subject to the use of the signals overlapping to QZSS and is therefore not supportable for BDS. In the future, the proposed AR method can be further refined by treating different-frequency and different-constellation biases jointly as DISBs. For example, to process DD measurements formed with signals QZSS L1 (1575.42 MHz) and BDS B1I (1561.098 MHz). Therefore, the proposed AR method can be expanded with any constellation transmitting code division multiple access signals.

Acknowledgements This work is supported by the Ministry of Science and Technology (Grant Nos. 109-2121-M-004-001- and 110-2221-E-004-004-MY3) of Taiwan and the GNSS Laboratory of Tokyo University of Marine Science and Technology (TUMST).

Data availability The test data used in this study can be available from the Geospatial Information Authority of Japan with an account (https://www.gsi.go.jp/).

References

Chu F-Y, Yang M, Wu J (2016) A new approach to modernized GPS phase-only ambiguity resolution over long baselines. J Geodesy 90(3):241–254

Chu F-Y, Ming Y, Chen Y-T (2019) GEO-pivoted carrier ambiguity resolution: a method for instantaneous ambiguity resolution in mid-low-latitude regions. GPS Solut 23:107

Cueto M, Magdaleno S, Cezon A, Sardon E (2012) Characterization of equatorial ionospheric features on the verge of the next solar cycle maximum. In: Proceedings: ION GNSS 2012, institute of navigation, Nashville, Tennessee, pp 3055–3065

Kubo N, Tokura H, Pullen S (2018) Mixed GPS–BeiDou RTK with inter-systems bias estimation aided by CSAC. GPS Solut 22:5

Li B, Verhagen S, Teunissen PJG (2014) Robustness of GNSS integer ambiguity resolution in the presence of atmospheric biases. GPS Solut 18(2):283–296

Li Q, Ma G, Maruyama T, Li J, Wan Q, Wang X, Fan J, Zhang J (2020) High-precision VTEC derivation with GEONET. Earth Planets Sp 72:14

Mi X, Zhang B, Yuan Y (2019) Multi GNSS inter system biases: estimability analysis and impact on RTK positioning. GPS Solut 23:81

National Space Policy Secretariat (2020) Quasi-Zenith Satellite System performance standard (PS-QZSS-002). National Space Policy Secretariat, Cabinet Office, Government of Japan

Odijk D, Teunissen PJG (2013) Characterization of between-receiver GPS-Galileo inter-system biases and their effect on mixed ambiguity resolution. GPS Solut 17(4):521–533
Odijk D, HvD M, Song I (2000) Precise GPS positioning by applying ionospheric corrections from an active control network. GPS Solut 3(3):49–57
Odijk D (2000) Weighting ionospheric corrections to improve fast GPS positioning over medium distances. In: Proceedings: ION GPS 2000 institute of navigation, SaltLake City, Utah, pp 1113–1123
Odolinski R, Teunissen PJG, Odijk D (2015) Combined BDS, Galileo, QZSS and GPS single-frequency RTK. GPS Solut 19(1):151–163
Odolinski R, Teunissen PJG, Odijk D (2014) Combined GPS+BDS+Galileo+QZSS for long baseline RTK positioning. In: Proceedings: ION GNSS+ 2014, institute of navigation, Tampa, Florida, pp 2326–2340
Strang G, Borre K (1997) Linear algebra, geodesy and GPS. Wellesley-Cambridge Press, Massachusetts
Teunissen PJG (1995) The least-squares ambiguity decorrelation adjustment: a method for fast GPS integer ambiguity estimation. J Geodesy 70(1–2):65–82
Teunissen PJG (1998) Success probability of integer GPS ambiguity rounding and bootstrapping. J Geodesy 72(1–2):606–612
Teunissen PJG (2001) Integer estimation in the presence of biases. J Geodesy 75(7):399–407
Teunissen PJG, Montenbruck O (2017) Handbook of global navigation satellite systems. Springer, Switzerland
Teunissen PJG, Verhagen S (2009) The GNSS ambiguity ratio-test revisited: a better way of using it. Surv Rev 41(312):138–151
Verhagen S, Li B (2012). LAMBDA software package. In: Matlab implementation, version 3.0, Delft University of Technology and Curtin University, Perth

Feng-Yu Chu is currently an assistant professor at the Department of Land Economics, National Chengchi University, Taiwan. Besides, he was a visiting researcher in TUMST from 2018 to 2019. His main expertise is GNSS precise positioning techniques, including navigation, RTK positioning, PPP, ambiguity resolution, software development, and related geodetic applications.

Nobuaki Kubo is a professor at the Tokyo University of Marine Science and Technology in the area of GPS/GNSS systems. He has been engaged in research and teaching of GNSS. Technical expertise and interests include high accuracy navigation using GNSS/IMU and sensors, in particular, algorithms and software developments for RTK-GNSS and some multipath mitigation techniques.

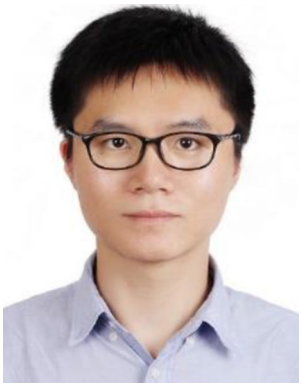

Yize Zhang is currently an associate professor at Shanghai Astronomical Observatory (SHAO). He received his Ph.D. degree from Tongji University in 2017. Then, he did his postdoctoral research at the Tokyo University of Marine Science and Technology (TUMSAT). His current research mainly focuses on multi-GNSS precise positioning and GNSS biases analysis.